Electrochimica Acta 146 (2014) 503–510

Contents lists available at ScienceDirect

Electrochimica Acta

journal homepage: www.elsevier.com/locate/electacta

High capacity and low cost spinel Fe_3O_4 for the Na-ion battery negative electrode materials

P. Ramesh Kumar, Young Hwa Jung, K. Kamala Bharathi, Chek Hai Lim, Do Kyung Kim *

Department of Materials Science and Engineering, Korea Advanced Institute of Science and Technology (KAIST), Daejeon 305-701, Republic of Korea

ARTICLE INFO

Article history:
Received 23 July 2014
Received in revised form 2 September 2014
Accepted 2 September 2014
Available online 22 September 2014

Keywords:
Fe_3O_4 nanoparticles
Na-ion battery
alginate binder
high capacity

ABSTRACT

The iron-containing electrode material is a promising candidate for low-cost Na-ion batteries. In this work, the electrochemical properties of Fe_3O_4 nanoparticles obtained by simple hydrothermal reaction are investigated as an anode material for Na-ion batteries. The Fe_3O_4 with alginate binder delivers a reversible capacity of 248 mAh g^{-1} after 50 cycles at a current density of 83 mA g^{-1} (0.1C), while the electrode using polyvinylidene fluoride binder shows a gradually capacity fading to 79 mAh g^{-1} after 50 cycles. The high electrochemical performance can be ascribed to both the nano size of Fe_3O_4 and excellent binding ability of alginate binder which can buffer large volume change. The mechanism of conversion reaction for Fe_3O_4 is also tracked by combining electrochemical impedance spectroscopy analysis and magnetization measurement after electrochemical cycling. Finally, the Na-ion full cell consisting of the Fe_3O_4-alginate anode and the $Na_3V_2(PO_4)_3$/graphene cathode is assembled to demonstrate performance of the Fe_3O_4 anode for Na-ion batteries.

1. Introduction

Lithium-ion batteries (LIBs) with an operating voltage of ~3.6–4 V have been extensively used as power sources for portable electronic devices such as laptops, cell phones, etc [1,2]. The lithium resources are limited which is main drawback to meet the large scale applications. Hence, it is necessary to develop the new batteries that can replace lithium such as sodium and magnesium-ion batteries [3–6]. The electrochemistry of sodium-ion batteries (SIBs) is almost similar to that of the LIBs. Furthermore, the cost of sodium-containing materials is relatively low due to the abundance of sodium resources. Therefore, SIBs could substitute current LIBs especially in large-scale energy storage applications. Whereas numerous materials have been investigated as cathode materials for SIBs, a few anode materials have been proposed [7]. Senguttuvan et al. reported the electrochemical properties of $Na_2Ti_3O_7$ with capacity of 175 mAh g^{-1} [8]. Sun et al. demonstrated high capacity Sb_2O_4 thin film electrode (896 mAh g^{-1}), but this material is concerned about poor safety [9]. Xiong *et al.* reported TiO_2 nanotube as an anode candidate for SIB's with capacity of 70 mAh g^{-1} [10]. Zhao *et al.* showed disodium terephthalate ($Na_2C_8H_4O_4$) as high performance anode material with stable capacity of 250 mAh g^{-1} [11]. Xiao *et al.* reported highly reversible alloying reactions in SnSb/C nanocomposites anode material with capacity of 544 mAh g^{-1} with good Coulombic efficiency [12]. Graphite cannot be used as an anode material for SIBs like LIBs due to the low intercalation/deintercalation capability of Na ions. Pure Na metal also cannot be used because of dendrite formation during continuous charging/discharging and low melting point which causes safety issues.

In this work, we present the high capacity and low cost Fe_3O_4 nanoparticles (< 10 nm) as an attractive candidate for a negative electrode material of SIBs. Ferrite (Fe_3O_4) is a ferrimagnetic material, crystalizes in inverse spinel structure with the space group of *Fd-3 m*. In inverse spinel structure, oxygen ions form face-centered cubic (FCC) lattice and the tetrahedral (A) sites are occupied by the Fe^{3+} ions and the octahedral sites (B) are occupied by the divalent metal ions Fe^{2+} and Fe^{3+}, in equal proportions [13,14]. In addition, Fe_3O_4 is a nontoxic and inexpensive material which can be obtained by easy synthetic process. Electrochemical activity of Fe_3O_4 in SIBs is firstly introduced by Komaba et al., as compared to electrochemical property of Li [15,16]. In 2013, Hariharan *et al.* demonstrated Fe_3O_4 nanoparticles as an anode material for both LIBs and SIBs based on conversion reaction [17]. Materials with nano dimensions (nanoparticles, nanorods, nanowires) have attracted enormous attention for their enhanced electrochemical properties and interesting behaviours applied in battery research field [15–20]. Due to high surface area and very fast redox reactions, battery capability and other electrochemical behaviours are highly influenced by nano materials. However, rechargeable batteries based on oxide anodes

* Corresponding author. Tel.: +82 42 350 4118; fax: +82 42 350 3310.
E-mail address: dkkim@kaist.ac.kr (D.K. Kim).

http://dx.doi.org/10.1016/j.electacta.2014.09.081
0013-4686/

generally suffer from low cyclability and low energy efficiency due to large polarization effects [21–25]. In addition to the particle size, binders used for electrode preparation have influenced on the electrochemical properties of ferrite anodes because the active materials are easily separated and isolated from the current collector and conducting agents by huge volume changes during conversion reactions. Especially, the volume expansion in SIBs can be intensified more than that in LIBs due to larger ionic radius of Na [16,26]. Effect of different binders (polyvinyl pyrrolidone (PVP), polyvinylidene fluoride (PVDF), poly acrylic acid (PAA) and carboxymethyl cellulose (CMC)) on electrochemical properties of electrodes have been reported by several research groups [27–31].

In the present case, we made an attempt to grow the Fe_3O_4 particles in sub 10 nm size and explored the possibilities to overcome the capacity fading problems in conversion reactions. Moreover, we have applied PVDF and alginate binders to explore the best binder for Fe_3O_4 anodes in SIBs for the first time to the best of our knowledge. In addition to that, we have performed the *ex-situ* magnetic studies on the electrodes during the electrochemical cycling, and we found that stable cycling performance and good rate capability of Fe_3O_4/alginate electrodes are correlated with the magnetic properties. Lastly, we assembled a sodium-ion full cell coupled with a cathode material, $Na_3V_2(PO_4)_3$, to confirm the feasibility of Fe_3O_4 nanoparticles for anode materials in SIBs.

2. Experimental details

2.1. Synthesis of Fe_3O_4 nanoparticles

Nanocrystalline Fe_3O_4 particles were synthesized by a hydrothermal method. 0.3244 gm of $FeCl_3$ was dissolved in 25 ml of deionized water under the vigorous magnetic stirring. 10 ml of 0.6 M Na_2CO_3 was added into the above solution drop by drop. After stirring the solution for 10 minutes, 0.12 gm of ascorbic acid was added into the solution and allowed for 20 minutes stirring. The suspension solution was transferred to a 100 ml teflon-lined container with 75% filling the volume of the autoclaves for hydrothermal reaction. The autoclaves were sealed and maintained at 160 °C for 3 h in a heating oven. After the reaction was complete, the autoclave was cooled down to room temperature. The final material was collected and washed with ethanol and deionized water several times to wash out the impurity ions, and then dried in an oven at 80 °C for few hours.

2.2. Characterization

Structural characterization at room temperature (RT) was performed by obtaining the powder X-ray diffraction (XRD) patterns employing Cu-Kα radiation (1.54 Å). The measurements were performed employing a PANalytical (X'pert PRO) X-ray diffractometer. Particle size and morphology analysis were characterized employing a field emission scanning electron microscope (FE-SEM Hitachi S-4800, Japan) and a transmission electron microscope with energy dispersive spectroscopy (TEM), JEOL 2010F HRTEM, Japan, with a 200 kV operating voltage. The Raman spectra of powders were recorded at RT employing a HR 800 Raman spectrophotometer (Jobin Yvon- Horiba, France) using monochromatic He-Ne LASER (633 nm), operating at 20 mW. Magnetization measurement was carried out at RT employing a vibrating sample magnetometer (VSM, LakeShore 7407).

2.3. Electrochemical measurement

The electrochemical studies of the synthesized Fe_3O_4 nanoparticle were conducted in a CR2032 coin cells. The composite electrode was prepared by mixing 70 wt. % of active material with 20 wt. % Super P carbon black and 10 wt. % PVDF and sodium alginate binders in suitable solvent. The obtained slurry was coated on a piece of copper foil and cut into 12 mm diameter circular electrodes. Sodium foil was used as an anode and 1 M solution of $NaClO_4$ in propylene carbonate was used as electrolyte. Coin cells were assembled in an argon-filled glove box (M. O. Tech, S. Korea) using borosilicate glass-fiber separator (Whatman GF/D). The $Na_3V_2(PO_4)_3$/G (G denotes

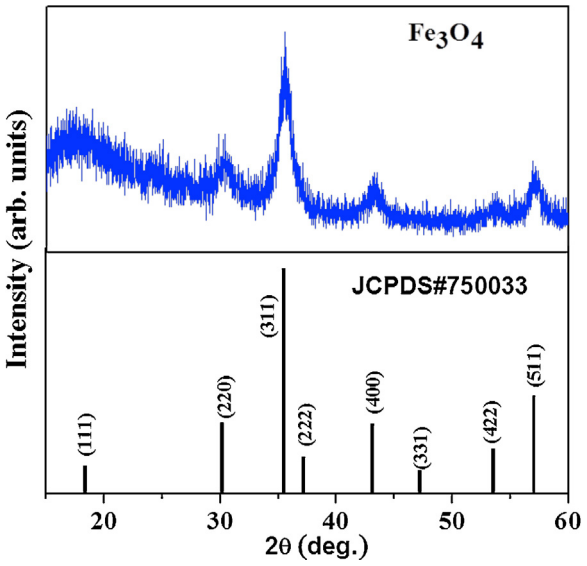

Fig. 1. The XRD pattern of Fe_3O_4 powders and formation of inverse spinel phase without any impurities is evident.

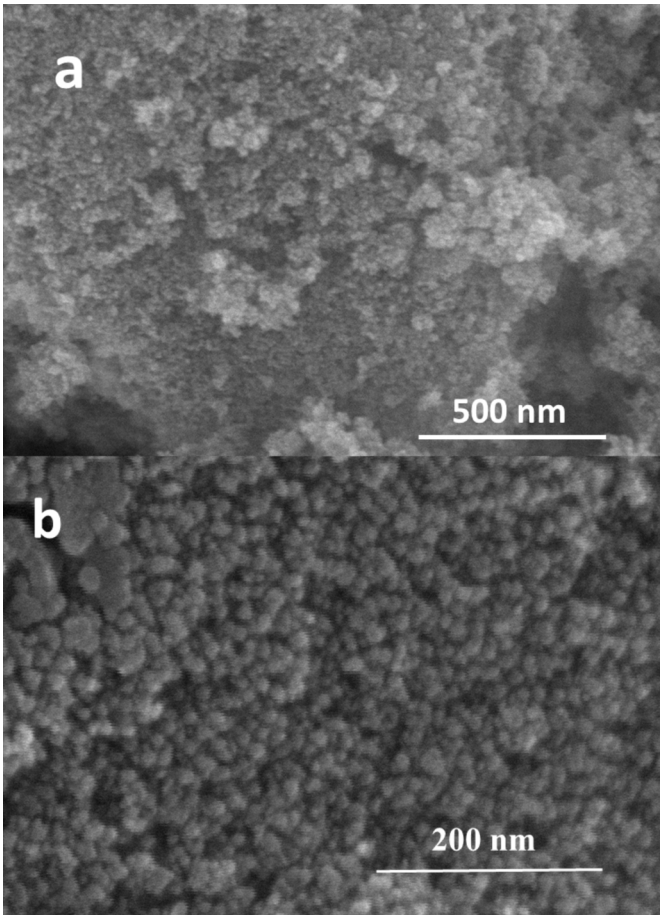

Fig. 2. SEM images of Fe_3O_4 particles. Uniform distribution of nano particles is clearly seen.

graphene) composite was used as a cathode material in testing Na-ion full cells. Details of the preparation and electrode fabrication for $Na_3V_2(PO_4)_3$/G are described in our previous paper [32]. We firstly assembled coin half-cells for Fe_3O_4/alginate electrodes with Na metal both to overcome large irreversible capacity and to confirm the capacity profile of the electrode again. We disassembled the coin cell after 5 cycles in the glove box, and washed the Fe_3O_4 electrode by pure DMC solvent three times. The electrode was dried in glove box for one day, and then the Na-ion full cell is made of a fresh-$Na_3V_2(PO_4)_3$/G electrode as a cathode and the pre-cycled Fe_3O_4 electrode as an anode. The mass loading for the cathode and the anode is 1 mg and 1.5 mg, respectively, and the area for the cathode and the anode is 1.13 cm^2 and 1.54 cm^2, respectively. The cyclic voltammetry and electrochemical impedance spectroscopy at various potentials during first discharge–charge cycle were measured using Biologic Science Instruments (Model: VMP3) between 1 M Hz to 2 m Hz under AC stimuli with 5 mV of amplitude. The Na-half cells were galvanostatically cycled between 3 V and 0.02 V using Automatic battery cycler system (WBCS3000, Wonatech, S. Korea), and the $Fe_3O_4/Na_3V_2(PO_4)_3$ Na-ion full cell was cycled between 3.2 V and 1.0 V at a rate of 0.2 C based on the cathode weight using a potentiostat (VMP3, Bio-Logic, France).

3. Results and Discussion

3.1. Structural characteristics and surface morphology

Fig. 1 shows the XRD patterns of the pure Fe_3O_4 powders recorded at room temperature. Fe_3O_4 is found to crystallize in inverse spinel structure belonging to *Fd-3m* space group without any impurity phase. The crystallite size (D) was calculated from the integral width of the diffraction lines using the well-known Scherrer's equation after background subtraction and correction for instrumental broadening.

The Scherrer equation is: $D=0.9\lambda/\beta\cos\theta$, where D is the size, λ is the wavelength of the filament used in the XRD machine, β is the width of a peak at half of its intensity, and θ is the angle of the peak [33]. The average grain size was found to be ~15 nm. Fig. 2 shows the SEM images of prepared Fe_3O_4 samples at different magnifications. From Fig. 2, the observed average particles size is 10 nm. The TEM images of the Fe_3O_4 nanoparticles shown in Fig. 3a and 3b indicate the formation of agglomerates with nanospheres ~10 nm in dia. Fig. 3c shows an HRTEM image of high crystalline Fe_3O_4 nanoparticles, and the inter-planar d-spacing is matched with the (220) and (311) planes for the inverse spinel Fe_3O_4 structure. From Fig. 3d, the observed Debye–Scherrer rings represent the (220), (311), (400), (511) and (440) lattice planes and confirm the phase and purity of Fe_3O_4 nanoparticles.

Fig. 4 shows the Raman spectra of Fe_3O_4 powder recorded at room temperature. Raman spectra showed five active modes of ($A_g + E_g + 3T_{2g}$) and the peaks were observed for Fe_3O_4 at 302.34 cm^{-1}, 460.38 cm^{-1}, 577.60 cm^{-1}, 615.88 cm^{-1} and at 690.63 cm^{-1}. The peaks corresponding to the wave numbers of 660 cm^{-1} to 720 cm^{-1} indicate tetrahedral group and that between 460 cm^{-1} to 660 cm^{-1} indicate octahedral group of ferrites [34].

3.2. Electrochemical characteristics for Na-half cells

Fig. 5a and 5b present cyclic voltammetry (CV) plots of Fe_3O_4 nanoparticles with PVDF and alginate binders for 20 scanning

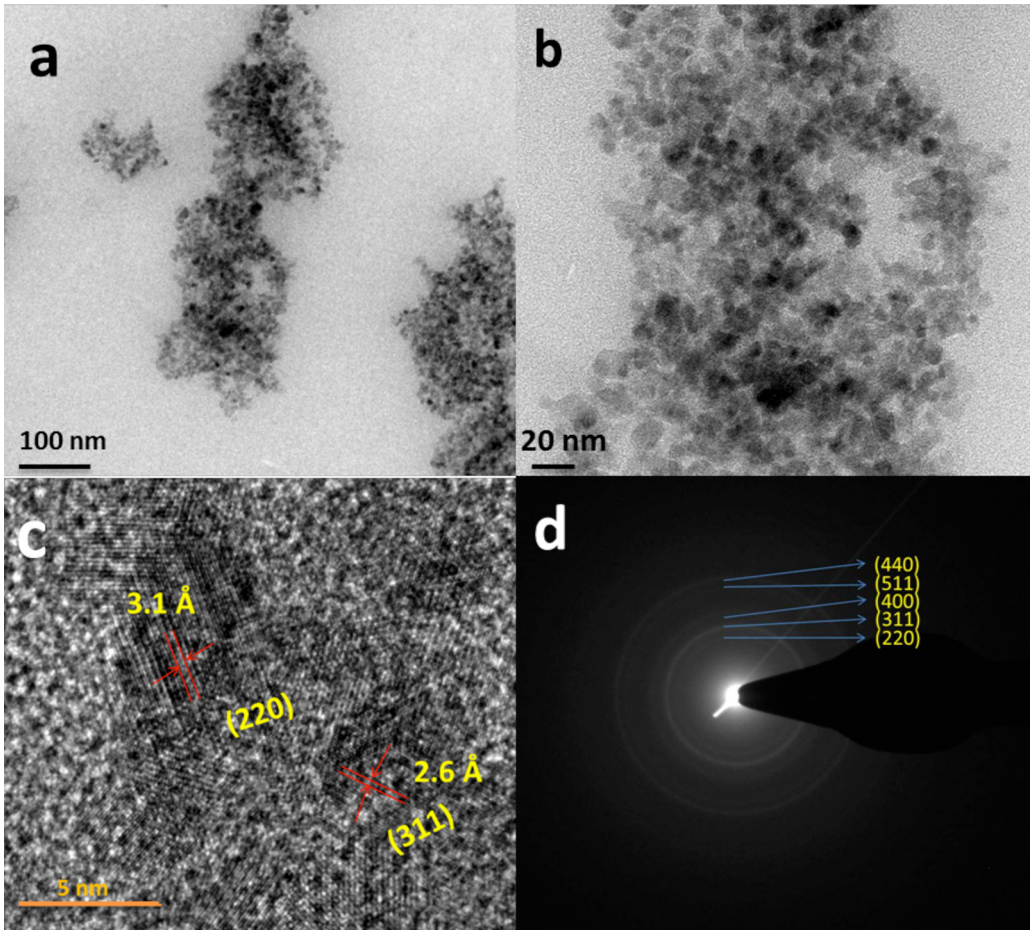

Fig. 3. (a) and (b) TEM images at different magnifications, (c) an HRTEM image, and (d) Debye–Scherrer ring patterns for Fe_3O_4 particles.

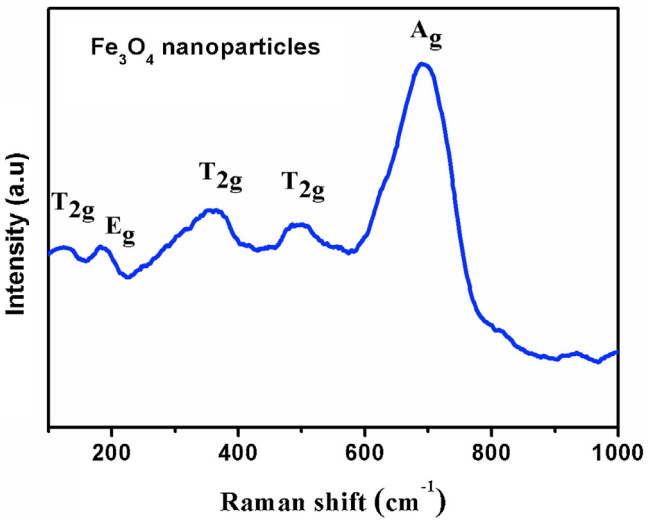

Fig. 4. Room temperature Raman spectra of Fe_3O_4 nanoparticles

cycles, respectively. From Fig. 5a and 5b, one cathodic peak at ~0.5 V is observed which corresponds to the conversion reactions of Fe^{2+}/Fe^{3+} to their metallic states and the formation of Na_2O [35]. The broad anodic peak around 1.5 V is ascribed to the oxidation reactions of metallic Fe. In Fig. 5, the redox peak intensity of Fe_3O_4 with alginate binder is gradually changed compared with the electrode using PVDF binder, which is indicating that higher electrochemical stabilities of electrode. These cyclic voltammetry results indicate that Fe_3O_4 with alginate binder exhibits better electrochemical properties than that with PVDF binder due to the high surface interaction between active materials and alginate binder.

Fig. 6 shows the cycling performance of Fe_3O_4 nanoparticles with PVDF binder. In Fig. 6a, Fe_3O_4 nanoparticles deliver an initial discharge capacity of 590 mAh g^{-1} at 83 mA g^{-1} (0.1C), and the discharge capacity value is 79 mAh g^{-1} after 50 cycles. Fig. 6b presents the discharge curves of Fe_3O_4 nanoparticles with PVDF binder up to 50 cycles. The cycling performance of Fe_3O_4 nanoparticles with alginate binder is shown in Fig. 7. From Fig. 7a, Fe_3O_4 nanoparticles with alginate binder maintained stable discharge capacity of 248 mAh g^{-1} after 50 cycles with 98% of Coulombic efficiency. The charge-discharge profile for the Fe_3O_4 nanoparticles with alginate binder for 50 cycles is represented in Fig. 7b. The discharge profile did not exhibit any significant plateau region, but rather a bump around 0.5 V, followed by a long tail, which contributed to almost 70% of the initial capacity. The alginate binder shows the considerable performance even in different high current rates. The discharge capacity at current rates of 834 mA g^{-1} (1C), 1668 mA g^{-1} (2C), 4170 mA g^{-1} (5C), 8340 mA g^{-1} (10C) and 16,680 mA g^{-1} (20C) for 10 cycles is shown in Fig. 8. The enhancement of electrochemical properties in Fe_3O_4 nanoparticles/alginate anode is might be due the strong bonding between nano crystalline material and binder.

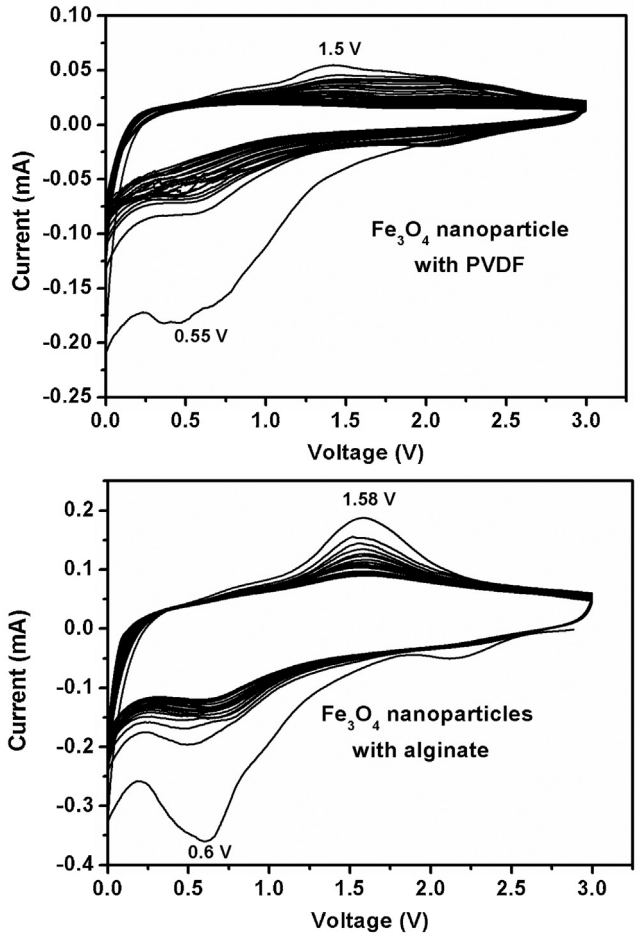

Fig. 5. Cyclic voltammetry plots for the Fe_3O_4 nanoparticles with PVDF and Na alginate binders

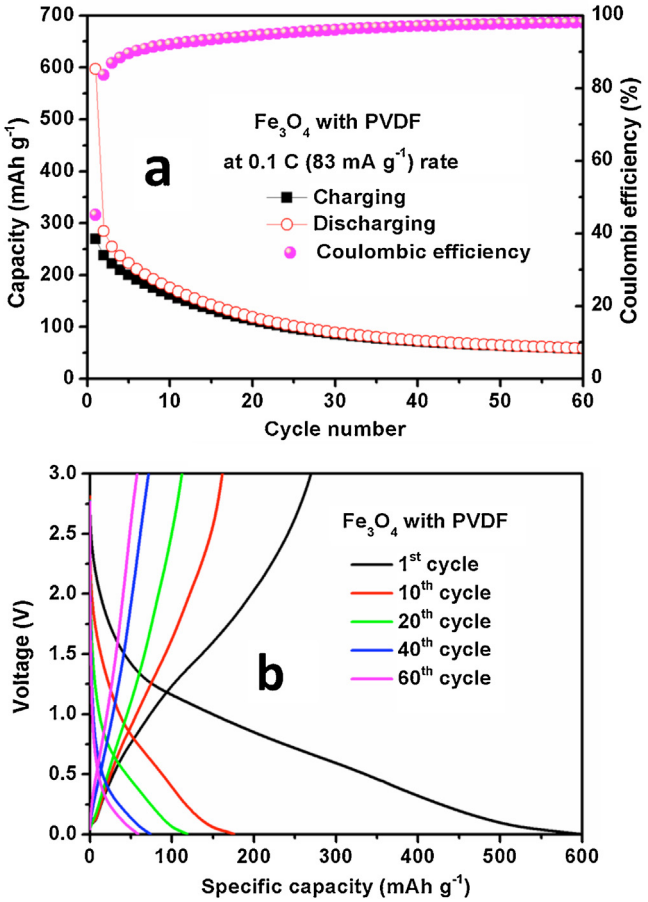

Fig. 6. (a) Cyclic performance and (b) charge/discharge plots for the Fe_3O_4 nanoparticles with PVDF binder at 0.1C rate.

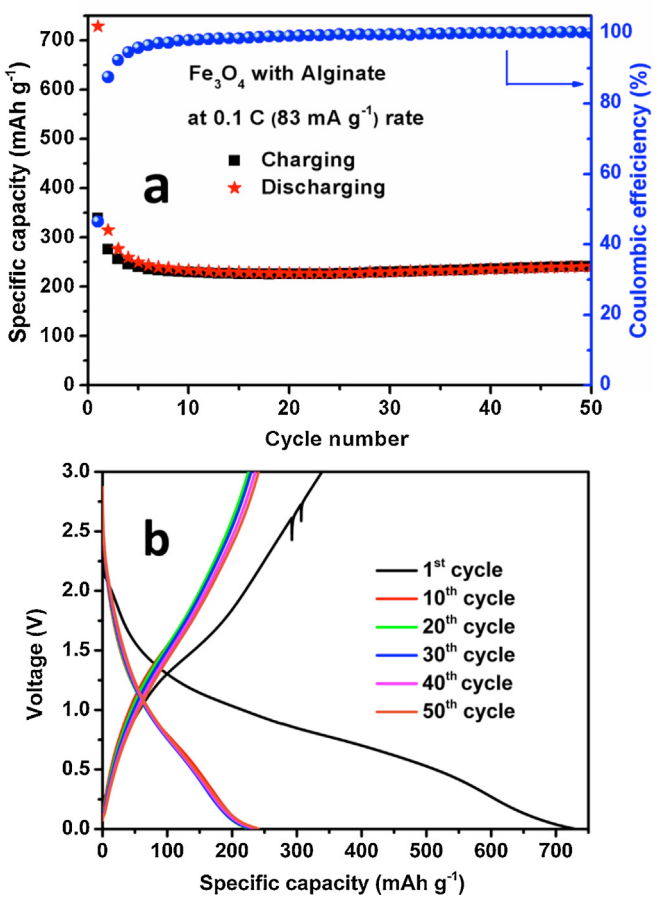

Fig. 7. (a) Cyclic performance and (b) charge/discharge plots for the Fe_3O_4 nanoparticles with Na-alginate binder at 0.1C rate.

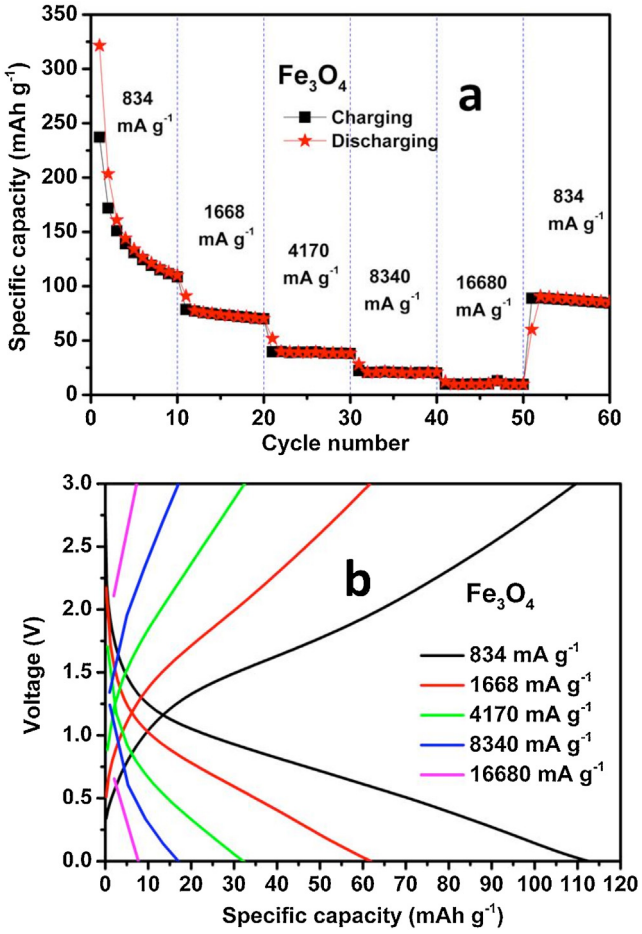

Fig. 8. (a) Cyclic performance and (b) charge/discharge plots for the Fe_3O_4 nanoparticles with Na-alginate binder at different current rates.

The scatters in Fig. 9 represent Nyquist plots for the Fe_3O_4 nanoparticles/alginate at different voltages. The latter were analyzed by fitting with an electrical equivalent circuit consisting of resistors and constant phase elements as shown in the inserted plot in Fig. 9a [36]. The electrical equivalent circuit elements are: electrolyte resistance (R_e), the inseparable surface film (SF) and charge transfer (CT) impedance $R_{(SF + CT)}$ and $CPE_{(SF+CT)}$ and the finite Warburg impedance (W_d).

In Fig. 9a, the impedance results for the Fe_3O_4 nanoparticles/alginate at discharging state showed one semicircle and one spike were observed in high and middle frequency range. The semicircle at higher frequency is related to the formation of passivation film on the surface (SF) and the charge transfer process at interface (CT). At OCV, only surface film contribution will occur and it is depending on concentration of electrolyte. In addition, solid electrolyte interphase (SEI) formation/partial dissolution/re-formation also takes place on cycling. This is reflected in the changes in the value of surface film impedance (RSF) up on cycling [37]. The values as per fitting are shown in Table 1.

The Nyquist plots of Fe_3O_4 nanoparticles/alginate anode during first charging state are shown in Fig. 9b. From Fig. 9b, at 0.6 V and 1.4 V, the Nyquist plots contain high frequency semicircle along with spike which is due to the formation of the metal oxides from the Fe-metal nano-particles through the conversion reaction. Further charging up to 2 V and 3 V, the surface film and charge transfer impedance decreases ascribed to partial dissolution of polymeric gel-type layer [38].

Therefore, a noticeable difference for the SEI formation and conversion processes existed for the sodiation of magnetite, matching with the above results. The specific capacity due to Fe_3O_4 sodiation was much lower than that predicted from Eq. (1), reinforcing the idea that a full conversion could not occur in this case. Furthermore, the volume change related to conversion reaction should also affect the cycling properties of the electrode which causes capacity fading. Hence, we concluded that the electrochemical impedance studies are supporting the conversion reaction mechanism.

3.3. Magnetic properties

Fe_3O_4 electrodes were prepared with PVDF and alginate binders separately and electrochemical cycling was performed on all of them. RT magnetic measurements were carried out on the Fe_3O_4 electrodes with alginate binder after the electrochemical cycling, due to their better electrochemical performance compared to that of Fe_3O_4/PVDF electrodes. Magnetization measurements were carried out on the electrodes after 1st discharge, 1st cycle, 10th cycle and 50 cycles. Fig. 10 shows the room temperature magnetization curves of Fe_3O_4/alginate electrodes compared to that of pure Fe_3O_4 powders. Magnetic moment is seen to be unsaturated even at 15 kOe for all the cases and the magnetic moment at 15 kOe is represented as saturation magnetization (M_S) here after. Saturation magnetization (M_S) of pure Fe_3O_4 powder is seen to be 87 emu g^{-1}, which is well matched with the previous reported values that indicating the formation of Fe_3O_4 in pure phase [39]. In the case of Fe_3O_4/alginate electrodes, saturation magnetization

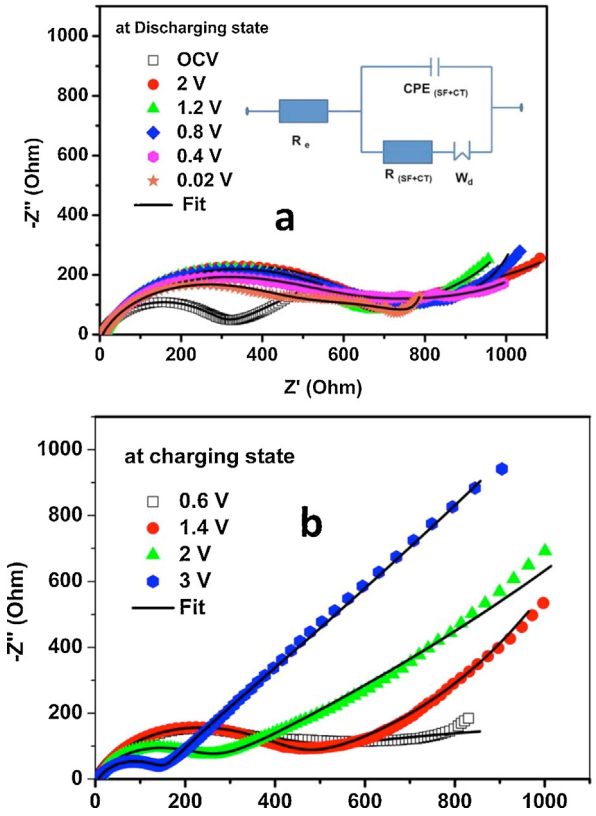

Fig. 9. Electrochemical impedance plots for the Fe_3O_4 nanoparticles with Na-alginate binder during (a) discharging and (b) charging.

values after 1st discharge, 1st cycle 10th cycle and 50th cycle are 64, 87, 37 and 41 emu g^{-1}, respectively (Table 2).

During the 1st discharge, Fe_3O_4 reacts with the Na ions and converts into Fe nanoparticles along with an amorphous Na_2O phase. However, in the reverse oxidation process (completion of 1st cycle), Fe nanoparticles are oxidized to Fe_3O_4 phases. Conversion redox mechanism may occur in the following steps [16]:

$$Fe_3O_4 + 8Na^+ + 8e^- \leftrightarrow 3Fe^0 + 4Na_2O \text{ ---- (1)} \quad (1)$$

M_s value after 1st discharge is seen to be 64 emu g^{-1} which is lower than that of pure Fe_3O_4 powders. M_s values after the electrochemical cycling can be explained as follows. After the 1st discharge, nanoparticle of Fe along with amorphous Na_2O is present in the electrode. Exchange interaction between the Fe magnetic moments might be complicated in the disordered discharged electrode due to the presence of amorphous Na_2O. Few moments might couple parallel to each other and few might couple anti-parallel to each other. Therefore, the net magnetization

Table 1
Impedance parameters of the Fe_3O_4 cell with an alginate binder during the 1st discharge–charge cycles at various voltages.

Voltage (V)	R_e (Ohm)	$R_{(SF+CT)}$ (Ohm)	W_d
Discharge OCV (2.8)	6.2	281	0.8
2	8.5	667	0.7
1.2	8.0	644	0.8
0.8	7.6	608	0.7
0.4	7.1	512	0.7
0.02	6.9	447	0.7
Charging 0.6	6.7	403	0.7
1.4	7.0	386	0.7
2	6.9	232	0.8
3	6.9	159	0.7

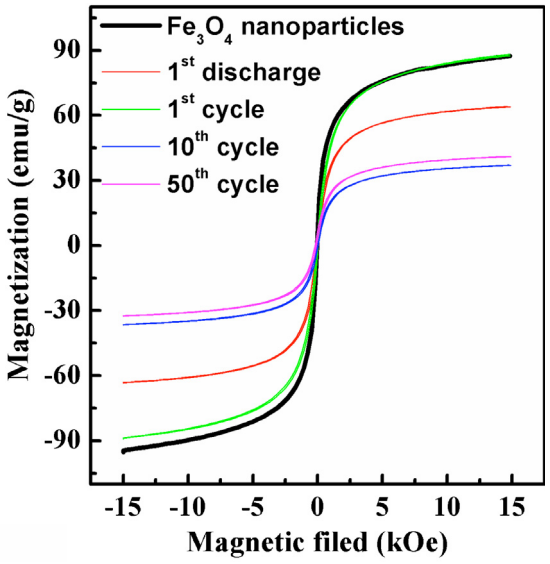

Fig. 10. Room temperature magnetization curves of Fe_3O_4-alginate electrodes after 1st discharge, 1st, 10th and 50th cycles compared with the pure Fe_3O_4 powders.

is expected to be less than the saturation magnetization value of pure Fe. Reported M_s value for pure Fe is 221 emu g^{-1} [40]. In addition to that, some of the Fe metal nanoparticles might have been converted into Fe oxides before the *ex-situ* magnetic measurement was carried out, leading to decrease in the saturation magnetization values. After the completion of 1st cycle, Fe nanoparticles are oxidized to Fe_3O_4. In the present case, the M_S value after 1st cycle is seen to be same as that of pure Fe_3O_4 powders, confirming the formation of Fe_3O_4 at charging state. After first cycle, M_S values are stable and its value is seen to be 41 emu g^{-1} after 50 cycles.

The saturation magnetization values are flowing same manner like discharge capacity values with number of cycles. Magnetization loops are seen to be very narrow after charging and discharging the electrodes. Due to the very small particle size, each particle behaves as a single domain resulted in superparamagnetic like behavior.

3.4. The $Fe_3O_4/Na_3V_2(PO_4)_3$ Na-ion full cell

The Na-ion full cell coupled with a $Na_3V_2(PO_4)_3$/G cathode was assembled to demonstrate feasibility of Fe_3O_4 nanoparticles with alginate binders as an anode material for real Na-ion battery system. Fig. 11a shows the cycling performance of a Fe_3O_4-alginate/$Na_3V_2(PO_4)_3$ full cell. The full cell delivers an initial discharge capacity of 92 mAh g^{-1} at a rate of 0.2C (1C corresponds 118 mAh g^{-1} based on theoretical capacity of a $Na_3V_2(PO_4)_3$ cathode), which is close to the reported practical capacity of $Na_3V_2(PO_4)_3$ [32]. The discharge capacity is decreased as 60 mAh g^{-1} after 20 cycles; however, charge/discharge efficiency has gradually increased by 99% from the initial efficiency of 94%. Although the cycling stability for a Na-ion full cell should be enhanced, this preliminary result indicates the feasibility of Fe_3O_4/alginate electrode as an anode for Na-ion batteries. Oh et al. reported the highest performance for Fe_3O_4 as an anode for Na-ion full cell; 76% of the initial capacity was achieved after 150 cycles for the $Fe_3O_4/Na[Ni_{0.25}Fe_{0.5}Mn_{0.25}O_2]$ full cell based on EMS electrolytes [35]. The practical capacity and cyclability of a full cell can be enhanced by optimizing other factors such as electrode formula and balance, electrolytes, and cell process conditions, thus, the future study will focus on performance improvement of Na-ion full cells considering these variables. The charge-discharge voltage profiles for the full cell

Table 2
Saturation magnetization values of Fe_3O_4- alginate electrodes after the electrochemical cycles.

Electrochemical cycles	Saturation magnetization (emu/g)Fe_3O_4-alginate electrode
1st discharge	64
1st cycle	87
10th cycle	37
50th cycle	41

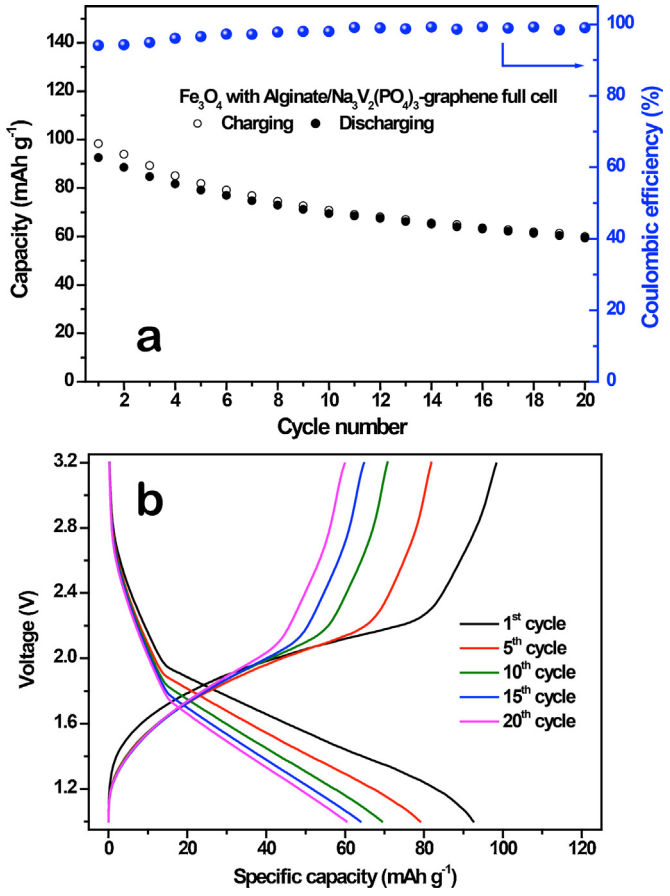

Fig. 11. (a) Cyclic performance and (b) charge/discharge plots for the Fe_3O_4-alginate/$Na_3V_2(PO_4)_3$/G Na-ion full cell at 0.2C rate in the voltage range from 1.0 to 3.2 V.

during cycling are presented in Fig. 11b. The Fe_3O_4-alginate/$Na_3V_2(PO_4)_3$/G full cell showed average discharging voltage of ~1.6 V, and the typical voltage profile is well matched with the voltage difference of $Na_3V_2(PO_4)_3$ and Fe_3O_4 half-cell results. The $Na_3V_2(PO_4)_3$ has shown a flat plateau at ~3.4 V vs. Na metal [32] while Fe_3O_4 exhibits rather a sloppy voltage profile as shown in Fig. 7b. Therefore, the overall profiles for the full cell follow anode side in this case.

4. Conclusions

Pure Fe_3O_4 nanoparticles were successfully synthesized by the hydrothermal process. The prepared Fe_3O_4 nanoparticles were characterized by XRD, Raman spectroscopy, SEM and HRTEM techniques. Electrochemical properties of Fe_3O_4 nanoparticles were investigated with two different binders (PVDF and Na-alginate), and Fe_3O_4 nanoparticles with alginate binder has delivered stable capacity of 248 mAh g^{-1} vs Na/Na^+ at 0.1C rate as well as good cyclability by 50 cycles. Furthermore, we have studied both electrochemical impedance and magnetization measurements for the Fe_3O_4/alginate electrode to find the path of conversion reaction mechanism during discharging and charging. Finally, we have confirmed possibility for real Na-ion full cells by combining a Fe_3O_4-alginate anode and $Na_3V_2(PO_4)_3$/G cathode. The current studies can expand understanding of conversion reaction in Na-ion batteries, and the iron-based nanoparticles with suitable binder system can be directly applied to realize low-cost Na-ion batteries for the foreseeable future.

Acknowledgements

Authors gratefully acknowledge financial support from the Program to Solve Climate Changes (NRF-2010-C1AAA001-2010-0029031) of Korea (NRF) funded by the Ministry of Science, ICT & Future Planning. This research was also supported by EEWS Research Project of the KAIST EEWS Initiative.

References

[1] N.S. Choi, Z.H. Chen, S.A. Freunberger, X.L. Ji, Y.K. Sun, K. Amine, G. Yushin, L.F. Nazar, J. Cho, P.G. Bruce, Challenges Facing Lithium Batteries and Electrical Double-Layer Capacitors, Angew. Chem. Int. Ed. 51 (2012) 9994–10024.
[2] J.B. Goodenough, Y. Kim, Challenges for Rechargeable Li Batteries, Chem. Mater. 22 (2010) 58–603.
[3] Y. Oumellal, A. Rougier, G.A. Nazri, J.M. Tarascon, L. Aymard, Metal hydrides for lithium-ion batteries, Nat. Mater. 7 (2008) 916–921.
[4] C.H. Lim, A.G. Kannan, H.W. Lee, D.K. Kim, A high power density electrode with ultralow carbon via direct growth of particles on graphene sheets, J. Mater. Chem. A 1 (2013) 6183–6190.
[5] S.W. Kim, D.H. Seo, X. Ma, G. Ceder, K. Kang, Electrode Materials for Rechargeable Sodium-Ion Batteries: Potential Alternatives to Current Lithium-Ion Batteries, Adv. Energy Mater. 2 (2012) 710–721.
[6] D. Kim, S.H. Kang, M. Slater, S. Rood, J.T. Vaughey, N. Karan, M. Balasubramanian, C.S. Johnson, Enabling Sodium Batteries Using Lithium-Substituted Sodium Layered Transition Metal Oxide Cathodes, Adv. Energy Mater. 1 (2011) 333–336.
[7] Y. Sun, L. Zhao, H. Pan, X. Lu, L. Gu, Y.-S. Hu, H. Li, M. Armand, Y. Ikuhara, L. Chen, X. Huang, A zero-strain layered metal oxide as the negative electrode for long-life sodium-ion batteries, Nature Commun. 4 (2013) 1–8.
[8] P. Senguttuvan, G. Rousse, V. Seznec, J.M. Tarascon, M.R. Palacin, $Na_2Ti_3O_7$: Lowest Voltage Ever Reported Oxide Insertion Electrode for Sodium Ion Batteries, Chem. Mater. 23 (2011) 4109–4111.
[9] Q. Sun, Q.Q. Ren, H. Li, Z.W. Fu, High capacity Sb_2O_4 thin film electrodes for rechargeable sodium battery, Electrochem. Commun. 13 (2011) 1462–1464.
[10] H. Xiong, M.D. Slater, M. Balasubramanian, C.S. Johnson, T. Rajh, Amorphous TiO_2 Nanotube Anode for Rechargeable Sodium Ion Batteries, J. Phys. Chem. Lett. 2 (2011) 2560–2565.
[11] L. Zhao, J. Zhao, Y.S. Hu, H. Li, Z. Zhou, M. Armand, L. Chen, Disodium Terephthalate ($Na_2C_8H_4O_4$) as High Performance Anode Material for Low-Cost Room-Temperature Sodium-Ion Battery, Adv. Energy Mater. 2 (2012) 962–965.
[12] L. Xiao, Y. Cao, J. Xiao, W. Wang, L. Kovarik, Z. Niea, J. Liu, High capacity, reversible alloying reactions in SnSb/C nanocomposites for Na-ion battery applications, Chem. Commun. 48 (2012) 3321–3323.
[13] C. Yang, J. Wu, Y. Hou, Fe_3O_4 nanostructures: synthesis, growth mechanism, properties and applications, Chem. Commun. 47 (2011) 5130–5141.
[14] Y. Wei, B. Han, X. Hua, Y. Lin, X. Wang, X. Deng, Synthesis of Fe_3O_4 Nanoparticles and their Magnetic Properties, Cryst. Growth Des. 5 (2005) 391–393.
[15] S. Komaba, T. Mikumo, A. Ogata, Electrochemical activity of nanocrystalline Fe_3O_4 in aprotic Li and Na salt electrolytes, Electrochem. Commun. 10 (2008) 1276–1279.
[16] S. Komaba, T. Mikumo, N. Yabuuchi, A. Ogata, H. Yoshida, Y. Yamada, Electrochemical Insertion of Li and Na Ions into Nanocrystalline Fe_3O_4 and α-Fe_2O_3 for Rechargeable Batteries, J. Electrochem. Soc. 157 (2010) A60–A65.
[17] S. Hariharan, K. Saravanan, V. Ramar, P. Balaya, A rationally designed dual role anode material for lithium-ion and sodium-ion batteries: case study of eco-friendly Fe_3O_4, Phy. Chem. Chem. Phys. 15 (2013) 2945–2953.

[18] D.K. Kim, P. Muralidharan, H.W. Lee, R. Ruffo, Y. Yang, C.K. Chan, H. Peng, R.A. Huggins, Y. Cui, Spinel $LiMn_2O_4$ Nanorods as Lithium Ion Battery Cathodes, Nano Lett. 8 (2008) 3948–3952.
[19] A.M. Tripathi, S. Mitra, Tin sulfide (SnS) nanorods: structural, optical and lithium storage property study, RSC Adv. 4 (2014) 10358–10366.
[20] C. Thomas Cherian, J. Sundaramurthy, M.V. Reddy, P. Suresh Kumar, K. Mani, D. Pliszka, C.H. Sow, S. Ramakrishna, B.V.R. Chowdari, Morphologically Robust $NiFe_2O_4$ Nanofibers as High Capacity Li-Ion Battery Anode Material, ACS Appl. Mater. Interfaces 5 (2013) 9957–9963.
[21] Z.M. Cui, L.Y. Jiang, W.G. Song, Y.G. Guo, High-Yield Gas-Liquid Interfacial Synthesis of Highly Dispersed Fe_3O_4 Nanocrystals and Their Application in Lithium-Ion Batteries, Chem. Mater. 21 (2009) 1162–1166.
[22] S. Ren, R. Prakash, D. Wang, V.S.K. Chakravadhanula, M. Fichtner, Fe_3O_4 Anchored onto Helical Carbon Nanofibers as High-Performance Anode in Lithium-Ion Batteries, ChemSusChem 5 (2012) 1397–1400.
[23] Y. Piao, H.S. Kim, Y.E. Sung, T. Hyeon, Facile scalable synthesis of magnetite nanocrystals embedded in carbon matrix as superior anode materials for lithium-ion batteries, Chem. Commun. 46 (2010) 118–120.
[24] E. Kang, Y.S. Jung, A.S. Cavanagh, G.-H. Kim, S.M. George, A.C. Dillon, J.K. Kim, J. Lee, Fe_3O_4 Nanoparticles Confined in Mesocellular Carbon Foam for High Performance Anode Materials for Lithium-Ion Batteries, Adv. Funct. Mater. 21 (2011) 2430–2438.
[25] Q.Q. Xiong, J.P. Tu, Y. Lu, J. Chen, Y.X. Yu, Y.Q. Qiao, X.L. Wang, C.D. Gu, Synthesis of Hierarchical Hollow-Structured Single-Crystalline Magnetite (Fe_3O_4) Microspheres: The Highly Powerful Storage versus Lithium as an Anode for Lithium Ion Batteries, J. Phys. Chem. C 116 (2012) 6495–6502.
[26] F. Klein, B. Jache, A. Bhide, P. Adelhelm, Conversion reactions for sodium-ion batteries, Phys. Chem. Chem. Phys. 15 (2013) 876–15887.
[27] N.S. Choi, Y.G. Lee, J.K. Park, Effect of cathode binder on electrochemical properties of lithium rechargeable polymer batteries, J. Power Sources 112 (2002) 61–66.
[28] Z. Wang, S. Madhavi, X.W. Lou, Ultralong α-MoO_3 Nanobelts: Synthesis and Effect of Binder Choice on Their Lithium Storage Properties, J. Phys. Chem. C 116 (2012) 12508–12513.
[29] I. Kovalenko, B. Zdyrko, A. Magasinski, B. Hertzberg, Z. Milicev, R. Burtovyy, I. Luzinov, G. Yushin, A Major Constituent of Brown Algae for Use in High-Capacity Li-Ion Batteries, Science 334 (2014) 75–79.
[30] P. Ramesh Kumar, S. Mitra, Nickel ferrite as a stable, high capacity and high rate anode for Li-ion battery applications, RSC Adv. 3 (2013) 25058–25064.
[31] M. Dahbi, T. Nakano, N. Yabuuchi, T. Ishikawa, K. Kubota, M. Fuunishi, S. Shibahara, J.-Y. Son, Y.-T. Cui, H. Oji, S. Komaba, Sodium carboxymethyl cellulose as a potential binder for hard-carbon negative electrodes in sodium-ion batteries, Electrochem. Commun. 44 (2014) 66–69.
[32] Y.H. Jung, C.H. Lim, D.K. Kim, Graphene-supported $Na_3V_2(PO_4)_3$ as a high rate cathode material for sodium-ion batteries, J. Mater. Chem. A 1 (2013) 11350–11354.
[33] A.L. Patterson, The Scherrer Formula for X-Ray Particle Size Determination, Phys. Rev. 56 (1939) 978–982.
[34] O.N. Shebanova, P. Lazor, Raman study of magnetite (Fe_3O_4): laser-induced thermal effects and oxidation, J. Raman Spectrosc. 34 (2003) 845–852.
[35] S.M. Oh, S.T. Myung, C.S. Yoon, J. Lu, J. Hassoun, B. Scrosati, K. Amine, Y.K. Sun, Advanced $Na[Ni_{0.25}Fe_{0.5}Mn_{0.25}]O_2/C$–$Fe_3O_4$ Sodium-Ion Batteries Using EMS Electrolyte for Energy Storage, Nano Lett. 14 (2014) 1620–1626.
[36] A. Zaban, E. Zinigrad, D. Aurbach, Impedance Spectroscopy of Li Electrodes. A General Simple Model of the Li-Solution Interphase in Polar Aprotic Systems, J. Phys. Chem. 100 (1996) 3089–3101.
[37] M.V. Reddy, T. Yu, C.H. Sow, Z.X. Shen, C.T. Lim, G.V. Subba Rao, B.V.R. Chowdari, α-Fe_2O_3 Nanoflakes as an Anode Material for Li-Ion Batteries, Adv. Funct. Mater. 17 (2007) 2792–2799.
[38] Y. Sharma, N. Sharma, G.V. Subba Rao, B.V.R. Chowdari, Studies on spinel cobaltites, $FeCo_2O_4$ and $MgCo_2O_4$ as anodes for Li-ion batteries, Sold state Ionics 179 (2008) 587–597.
[39] Y. Hou, J. Yu, S. Gao, Solvothermal reduction synthesis and characterization of superparamagnetic magnetite nanoparticles, J. Mater. Chem. 13 (2003) 1983–1987.
[40] S. Arajs, G.R. Dunmyre, A Note on the Consistency of Values of the Spontaneous or Saturation Magnetization of Polycrystalline Iron and Nickel at 298 K, phys. stat. sol. (b) 21 (1967) 191–195.